energies

MDPI

Article

Experimental Study on Microscopic Water Flooding Mechanism of High-Porosity, High-Permeability, Medium-High-Viscosity Oil Reservoir

Yang Li [1,2], Pin Jia [1,2,*], Ming Li [1,2], Haoran Feng [1,2], Cong Peng [1,2] and Linsong Cheng [1,2]

1 State Key Laboratory of Petroleum Resources and Prospecting, China University of Petroleum (Beijing), Beijing 102249, China; 2021210264@student.cup.edu.cn (Y.L.); lm151299427@163.com (M.L.); 2022210271@student.cup.edu.cn (H.F.); 2022210272@student.cup.edu.cn (C.P.); lscheng@cup.edu.cn (L.C.)
2 College of Petroleum Engineering, China University of Petroleum (Beijing), Beijing 102249, China
* Correspondence: jiapin1990@163.com

Abstract: After the development of high-porosity, high-permeability, medium-high-viscosity oil reservoirs enters the high-water-cut stage, the remaining oil is highly dispersed on the microscopic scale, which leads to a change in the oil-water-flow law. If the enrichment and mobilization laws of the microscopic remaining oil cannot be truly and objectively described, it will ultimately affect the production of oil fields. At present, few studies have directly revealed the microscopic water flooding mechanism of high-porosity, high-permeability, medium-high-viscosity oil reservoirs and the main controlling factors affecting the formation of remaining oil. Starting with micro-physical simulation, this study explores the water flooding mechanism on the microscale, the type of remaining oil and its evolution law, and analyzes the main controlling factors of different types of remaining oil so as to propose effective adjustment and development plans for different types of remaining oil. It is found that this type of reservoir has a serious jet filtration phenomenon in the early stages of water flooding and is accompanied by the penetration of injected water, detouring flow, pore wall pressing flow, the stripping effect, and the blocking effect of the rock skeleton. The remaining oil is divided into five types: contiguous flake shape, porous shape, membrane shape, striped shape, and drip shape. Among them, the transformation of flake-shape and porous-shape remaining oil is greatly affected by the viscosity of crude oil. The decrease effect of crude oil viscosity on contiguous residual oil was as high as 33.7%, and the contiguous residual oil was mainly transformed into porous residual oil. The development of membrane-shape, striped-shape, and drip-shape remaining oil is more affected by water injection intensity. The decrease in water injection intensity on membrane residual oil was as high as 33.3%, and the membrane residual oil shifted to striped and drip residual oil. This paper classifies remaining oil on the microscopic scale and clarifies the microscopic water flooding mechanism, microscopic remaining oil evolution rules, and the main controlling factors of different types of remaining oil in high-porosity, high-permeability, medium-high-viscosity oil reservoirs.

Keywords: high-porosity high-permeability medium-high-viscosity oil reservoir; microfluidics; water flooding mechanism; remaining oil type

Citation: Li, Y.; Jia, P.; Li, M.; Feng, H.; Peng, C.; Cheng, L. Experimental Study on Microscopic Water Flooding Mechanism of High-Porosity, High-Permeability, Medium-High-Viscosity Oil Reservoir. *Energies* **2023**, *16*, 6101. https://doi.org/10.3390/en16176101

Academic Editor: Roland W Lewis

Received: 21 July 2023
Revised: 10 August 2023
Accepted: 14 August 2023
Published: 22 August 2023

1. Introduction

High-porosity, high-permeability reservoirs generally have the characteristics of strong edge-bottom water energy [1]. After a long period of development, they have entered the stages of high water cut and extra high water cut. The BZ oilfield is a typical high-porosity, high-permeability reservoir. After entering the high water cut stage, the reservoir is full of water, but the recovery degree is low. Macroscopically, there is little room for improvement in the water sweep degree. This research will study the enrichment and mobilization of remaining oil in the reservoir from a microscopic perspective. The microscopic water flooding mechanism in the development process has an important guiding role in improving oil recovery and, especially, achieving economical and efficient development of high-porosity, high-permeability, medium-high-viscosity oil reservoirs.

In recent years, with the rapid development of microfluidic technology, scholars worldwide have introduced it into the field of petroleum engineering and carried out fundamental theoretical research on oil and gas field development. A series of achievements have been made in the study of oil-gas-water fracture-matrix seepage law and oil recovery enhancement with chemical flooding on the microscale, which provides theoretical guidance for the application of microfluidic technology in the field of oil and gas field development. Alfred Chatenever et al. [2] firstly used the granular filling microscopic glass model to carry out the visualization study of microscopic water drive characteristics, focusing on the analysis of the water drive process and microscopic remaining oil formation mechanism. Guo [3] studied the oil mobilization mechanism of water flooding by using a microfluidic model and the water flooding law on the pore scale. With the development of microfluidic technology, microfluidic model materials have gradually expanded from silicon wafers to glass, quartz, and polymer materials [4–8]. At the same time, real core slices are also used as microfluidic models in the area of oil and gas field development. Zhou et al. [9] used the glass microfluidic model to study the mechanism of water flooding and clarify the effects of different fracture characteristics on the law of water flooding in fractured reservoirs. Chen Yingying et al. [10] used the visual fracture model to study the influence of displacement speed, model dip angle, and other factors on the oil mobilization degree. The results show that there is an optimal displacement speed for water flooding that achieves maximum oil mobilization while avoiding water channeling. Water flooding is mainly affected by reservoir wettability, fracture connectivity, and gravity differentiation. Chen [11] carried out microfluidic experiments on sandstone models, conglomerate models, and four types of reef limestone models. It was found that the matrix had a great influence on the effective mobilization of fluids in reef limestone. The remaining oil in the sandstone model and conglomerate model is mainly presented as the oil film and spot, while the remaining oil in the reef limestone model is mainly presented as the oil film attached to the pore-fracture surface. Alizadeh et al. [12] carried out microfluidic experimental research on the interaction of crude oil, carbonated water, and carbon dioxide gas in the process of carbonated water flooding. It was found that in the process of carbonated water flooding, with the outlet back pressure dropping, carbon dioxide is gradually released from the carbonated water, forming a carbonated water-crude oil-carbon dioxide dual displacement mechanism including internal gas displacement, carbonated water flooding, gas diffusion displacement, etc., which can effectively enhance oil recovery and increase the sequestration amount of carbon dioxide. Chen Xinglong et al. [13] used microfluidic technology to study the water-flooding oil mobilization in the dead-end pores and found that the water flooding process was difficult to mobilize the crude oil in the dead end, and the main mobilization positions were the mainstream channel and the dead-end inlet. The mobilization process can be divided into three stages: the main channel emptying stage, the elastic oil change stage, and the ineffective water injection stage. Cui et al. [14] revealed the influence of depletion development and water injection development on oil mobilization under high-temperature and high-pressure conditions. By comparing the water flooding mobilization after depletion and that before depletion, according to the microfluidic model, it is found that the remaining oil adjusted to the water flooding experiment after depletion development is less and the color is darker, indicating that the light component escapes during depletion development. The proportion of heavy components in the remaining oil increases, and the released natural gas carries crude oil to the output. At the same time, the released dissolved gas produces a jamming effect in the pores and occupies part of the pore volume. With the continuous injection of water, the injected water first mobilizes the oil in the large pores, and the oil in the small pores is difficult to mobilize, so the contiguous remaining oil is accumulated. Junjian Li and many other scholars also conducted a large number of studies on the occurrence and state of microscopic remaining oil. According to the topological structure and other characteristics of microscopic remaining oil, it was divided into five types: cluster, porous, columnar, droplet, and membrane, and their dynamic evolution laws were studied [4,15]. Chuan Wang et al. studied the flow law of oil and water at the ultra-high water cut stage and analyzed its flow path, further improving and developing the existing research theory of microscopic remaining oil based on the previous research results of microscopic remaining oil classification and using indoor physical experiments and statistical mathematics as the main research methods [16].

Microfluidic technology is of great significance to the study of the visual and physical simulation of multiphase flow. It can visually present the flow characteristics of oil and water [17,18]. It is direct with microfluidic technology to observe the distribution of microscopic remaining oil and the degree of water-flooding oil mobilization. By designing the pore throat size of the microfluidic model, the distribution and migration characteristics of fluid at a specific scale can be clarified.

After the development enters the high water cut stage, the remaining oil is highly dispersed on the microscale, which will inevitably lead to a change in the oil-water-flow law. If the enrichment and mobilization laws of microscopic remaining oil cannot be objectively clarified, it will ultimately affect the enhancement of oil production. At present, few studies have directly revealed the microscopic water flooding mechanism of high-porosity, high-permeability, medium-high-viscosity oil reservoirs and the main controlling factors affecting the formation of remaining oil. Starting with micro-physical simulation, this study explores the water flooding mechanism on the microscale, classifies the remaining oil and reveals its evolution law, and analyzes the main controlling factors of different types of remaining oil so as to propose effective adjustment plans for exploiting different types of remaining oil. This study deeply clarifies the microscopic water flooding mechanism of high-porosity, high-permeability, medium-high-viscosity oil reservoirs and the main controlling factors for exploiting different types of remaining oil, and proposes advice for tapping the reservoir potential, which has important guiding significance for improving reservoir recovery.

2. Microfluidic Physical Simulation Method

2.1. Experimental Equipment

The experimental equipment mainly includes: a vertical single-cylinder pump, intermediate vessel sets, a visualization clamping kettle, an in-body microscope, and a visualizer. The experimental equipment is shown in Figure 1. Specific equipment parameters are shown in Table 1.

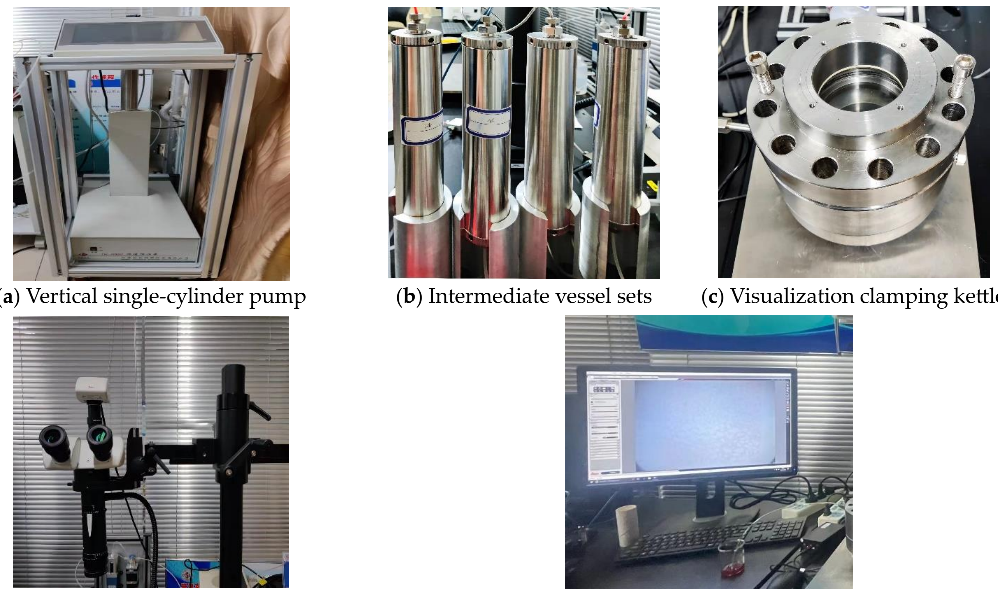

(**a**) Vertical single-cylinder pump (**b**) Intermediate vessel sets (**c**) Visualization clamping kettle

(**d**) In-body microscope (**e**) Visualizer

Figure 1. Main equipment for microfluidic experiments.

Table 1. Experimental equipment parameters.

Equipment Name	Equipment Type	Main Parameters of the Equipment
Vertical single-cylinder pump	TC-100D	Withstanding pressure 60 MPa; pressure accuracy 0.1% FS; Flow rate range 0.01–30 mL/min; single pump volume 100 mL
High-pressure intermediate vessel sets	ZJ-100	Pressure resistance 60 MPa; Temperature resistance 150 °C; Vessel volume 100 mL; resolution 0.01 mL
In-body microscope	Leica Z16APO	Zoom 16:1; Main unit zoom range 0.57X–9.2X; Magnification 7.1X–115X; Maximum optical magnification 920X; Maximum resolving power 336 lp/mm; Large range of activity distance 97 mm
Visualization clamping kettle	HD1	Pressure-resistant 60 MPa; temperature-resistant 150 °C; Can be covered with half-open heating jacket, half-open heat preservation sleeve, temperature control by electric heating and connected to the pressure and temperature monitoring system

Aiming at the reservoir characteristics of the high porosity and high permeability of the BZ reservoir and the fluid characteristics of crude oil with a large viscosity span, a microscopic experimental physical simulation method of a high porosity and high permeability reservoir is formed in terms of both an experimental model and experimental fluid. The fluid properties of the crude oil are analyzed, and then the configuration of the oil for the simulation is completed. Design the microfluidic model based on the typical cast sheet photographs of the BZ reservoir and characterize the pore throat to carry out the microfluidic experimental research.

2.2. Experimental Material

The BZ reservoir, on which this study is based, is a typical narrow-channel reservoir with high porosity and high permeability within the channel (35% porosity and 2000 mD permeability).

2.2.1. Fluid Simulation Methods

This experiment is to simulate the real underground water drive process. According to the real fluid parameters of the BZ reservoir, the simulated oil and replacement fluid needed for the experiment are configured in the following manner.

Experimental oil: The simulated oil used in this experiment is a compound oil made of anhydrous kerosene and motor oil mixed proportionally. The viscosity of the compound oil is 20 mPa·s, the density is 0.85 g/cm^3, and it is dyed red with Sudan III dye. The viscosity of kerosene is 2.5 mPa·s, the density is 0.8 g/cm^3, the freezing point is −47 °C, the boiling range is 180–310 °C, and its average molecular weight is between 200–250. The viscosity of motor oil is 150 mPa·s, its density is 0.88 g/cm^3, the freezing point is −37 °C, the boiling range is 200–300 °C, and the average molecular weight is between 150–400.

Experimental water: The repellent used in this experiment was distilled water, dyed blue with methyl blue stain. The viscosity of distilled water is 1 mPa·s, the density is 1 g/cm^3, the freezing point is 0 °C, the boiling point is 100 °C, and the molecular weight is 18.

2.2.2. Reservoir Simulation Methods

On the basis of a thorough investigation of the physical simulation methods of the water drive, the design and fabrication of the micro-experimental model are carried out with reference to the physical parameter indicators of the experimental prototype BZ reservoir. In terms of microfluidic modeling, the etched glass model was designed and fabricated based on the typical cast thin section photos of the BZ reservoir. The cast thin section photo of well F16 is selected as the benchmark unit for the pore and howl channel, as shown in Figure 2. The test results for the cast thin section are shown in Table 2.

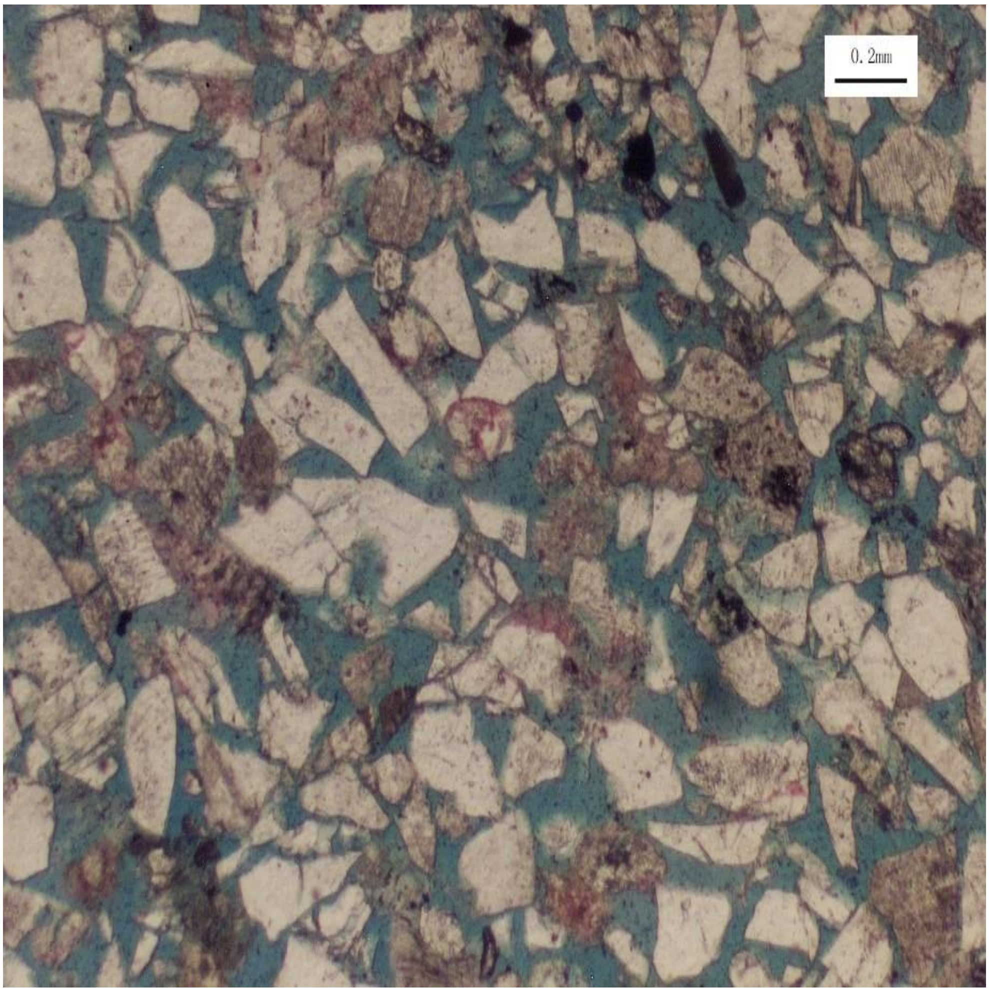

Figure 2. Photograph of a thin section of well F16 core cast body.

Table 2. Results of cast thin section testing.

Sample Number	Maximum/Major Particle Size Range (mm)	Sorting	Composition of Structural Particles (%)				GAP-Filler		Plane Porosity	
			Quartz	Feldspar	Rock Waste	Else	Matrix	Cement	Intergranular Pore	Intragranular Pore
1-001A	0.52/0.15~0.35	medium	38	46	13.5	2.5	1	0.5	28	3

The rock pores in the flakes are well developed and connected, mainly dissolved intergranular pores and primary pores, with pore diameters generally ranging from 0.15 to 0.4 mm, and some feldspars and clasts have developed intragranular pores; a small number of particles (e.g., feldspars, acidic ejecta, kyanite, gneisses, and other clasts) have been intensely dissolved and honeycombed or are only remnants of them. The connectivity of the rocks is locally affected by the presence of fine grains and pseudomagmatic or extruded mica or plastic rock fragments.

The rock skeleton and pore throats were binarized based on cast thin-section photographs, and the extracted pore throats are shown in Figure 3. Microscopic glass etching was performed, and the experimental model is shown in Figure 4. The size of the microfluidic model etching area in the experiment is 30 × 30 mm, and the etching depth is 0.035 mm.

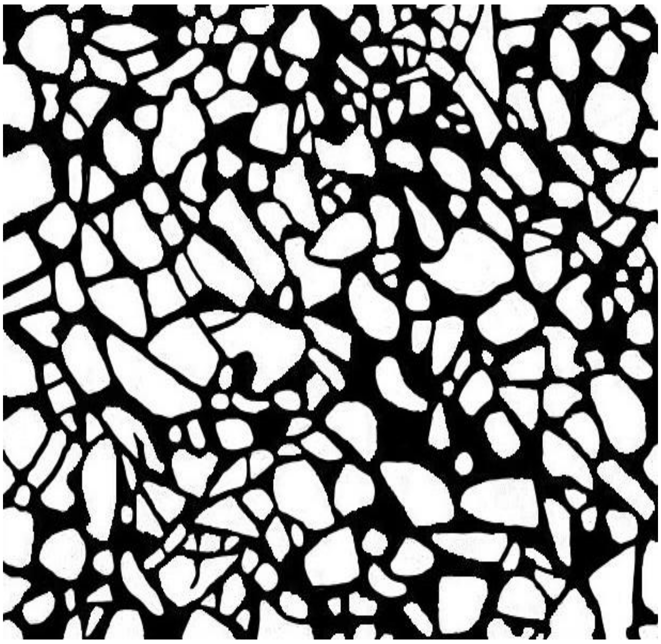

Figure 3. Numerical model of rock skeleton and pore throat.

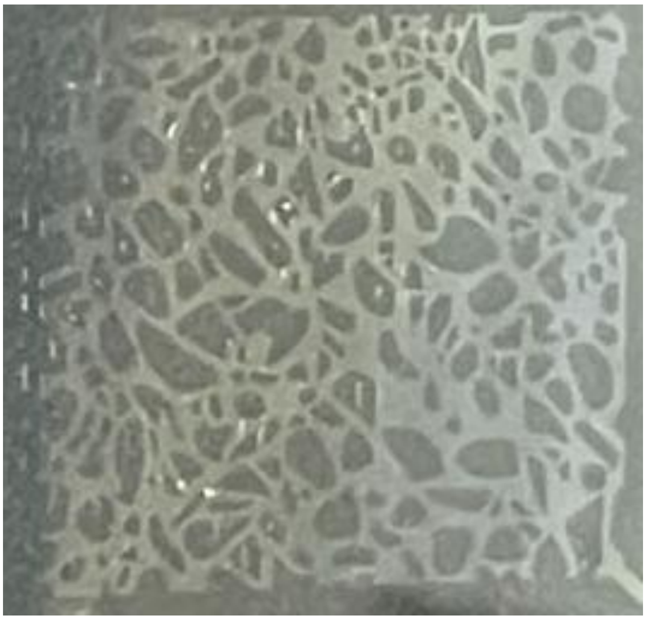

Figure 4. Microfluidic etching glass model.

3. Microfluidic Water Drive Experimental Design and Procedure

Microfluidic experiments can truly and completely present the water-driven oil process at the pore-throat scale and can visually present water-driven characteristics and residual oil mobilization characteristics.

3.1. Experimental Programme Design

In order to clarify the microscopic water drive mechanism and the main controlling factors of microscopic residual oil formation in high-porosity and high-permeability thick oil reservoirs, three groups of microfluidic experiments were designed in this study. The specific experimental parameters are shown in Table 3.

Table 3. Microfluidic experiment design scheme.

Serial Number	Modeled Permeability (md)	Crude Oil Viscosity (mPa·s)	Filling Rate (mL/min)	Injection-Production Direction	Research Purpose
1	2000	20	0.02	Diagonal injection and production	Basic program
2	2000	2	0.02	Diagonal injection and production	Exploring the effect of crude oil viscosity on water drive effectiveness
3	2000	20	0.06	Diagonal injection and production	Exploring the effect of injection rate on water drive effect

3.2. Experimental Procedure and Steps

3.2.1. Experimental Procedure

The microfluidic experimental platform is built with the above equipment to form a set of experimental flows applicable to microscopic water drive physics simulation experiments. The experimental flow chart is shown in Figure 5. The experimental platform is mainly composed of an injection system, a visualization clamping kettle, and an image acquisition and analysis system. The injection system mainly includes the TC-100D vertical single-cylinder pump and high-pressure piston intermediate vessel set. The image acquisition and analysis system includes a Leica Z16APO body microscope, a high-speed video camera, and computer-aided equipment to record the water-driven dynamics of the microfluidic model in real time.

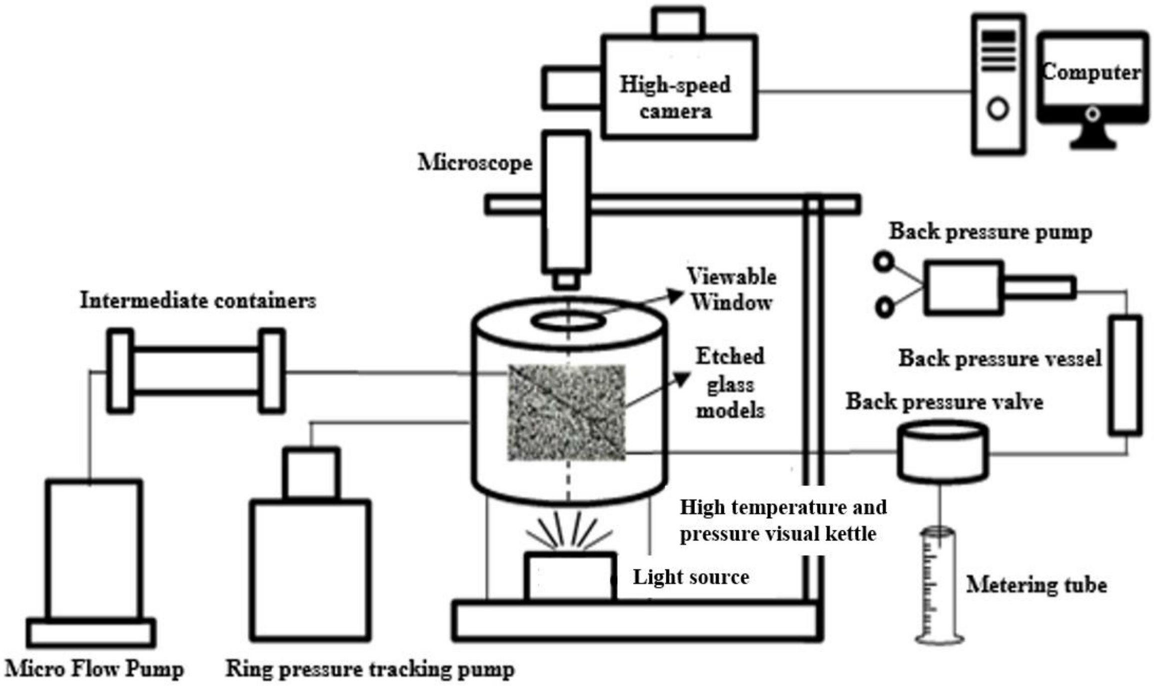

Figure 5. Flowchart of microfluidic experiment.

3.2.2. Experimental Steps

① Pipeline design and connection

According to the experimental process (the production of a number of different lengths of pipeline) due to the microscopic experiments on the fluid volume being more sensitive, this experiment uses a transparent plastic hose with a diameter of 3 mm to facilitate the observation of fluid flow. A number of connectors (six, three) and control valves will be connected to the different equipment to form a complete pathway.

② Preparation and assembly of experimental oil

According to the experimental program, this experiment uses the viscosity of 20 mPa·s and 2 mPa·s compound oil, of which the allocation ratio of 20 mPa·s oil kerosene and engine oil is 4:7 and the allocation ratio of 2 mPa·s oil kerosene and engine oil is 5:1; the use of automatic rotational viscometer measurement to check the configured simulated oil to ensure the viscosity accuracy; the use of Sudan III bio-dyeing agent for simulated oil dyeing and filtering; the simulated oil assembled into the intermediate container.

③ Experimental water preparation and assembly

The appropriate volume of distilled water was poured, stained, and filtered using methyl blue dye, and the stained simulated water was assembled into the corresponding intermediate containers.

④ Assembly of hydrophobic agent and anhydrous ethanol

Appropriate volumes of hydrophobic agent (N-ethyl-N-benzylaniline) and anhydrous ethanol were poured, filtered, and assembled into the corresponding intermediate containers, respectively.

⑤ Etched glass model assembly

The etched glass model used in the experiment was assembled into the visualization gripper, the screws were tightened evenly to prevent the model from rupture due to uneven stress, the height of the eyepiece of the microscope and the magnification were adjusted so that the etched area of the glass model was presented in the field of view in its entirety, and the saturation, contrast, and gamma values of the image acquisition system were adjusted so as to make the model's contour and color clear.

⑥ Saturated hydrophobic

Open the switch corresponding to the hydrophobic agent, with a vertical single-cylinder pump at a speed of 0.1 mL/min model saturation, until the model is full of hydrophobic agent and out of the outlet end. Turn off the switch, saturated with 24 h of rest to fully change the model's wettability, so that the model inside the hole throat wall is lipophilic.

⑦ Saturated oil

Turn on the analog oil corresponding switch, saturate the model with oil using a single-cylinder pump at 0.02 mL/min. When the model is full of oil and there is analog oil flowing out of the outlet end, turn off the switch and take a picture with an image acquisition system.

⑧ Water-driven oil

Turn on the image acquisition system camera, turn on the analog water corresponding to the switch, with a single-cylinder pump at a speed of 0.02 mL/min water drive to the model, until the remaining oil in the model does not change and the outlet end of the water content is 100% to stop the water drive; turn off the camera and the microscopic residual oil in the whole domain and the local photo.

⑨ Model cleaning

Anhydrous ethanol and hydrophobic agents were successively used to displace the remaining fluid in the model with a single-cylinder pump at a rate of 0.1 mL/min, and the model orifice throat was cleaned for the next set of experiments.

4. Analysis of Experiment Results

4.1. Water Flooding Characteristics and Mechanism on the Microscale

According to the experimental scheme, the basic scheme simulation is carried out first. The permeability of the etched glass model is 2000 mD, the viscosity of the simulated oil is 20 mPa·s, and the water injection rate is 0.02 mL/min. The characteristics and mechanisms of microscopic water flooding and the evolution law of microscopic remaining oil are analyzed as follows:

4.1.1. Water Flooding Characteristics on the Microscale

In the early stages of water flooding, the injected water is filiform along the line between injection and production wells. As the displacement progresses, the injected water diffuses along the main stream line to the unswept areas on both sides. After the water is seen at the outlet end, the spread of the injected water reaches almost 100%. At the end of water flooding, the shape and content of the remaining oil hardly change with the change in injection volume. The experiment is over. The process of the water flooding experiment is shown in Figure 6.

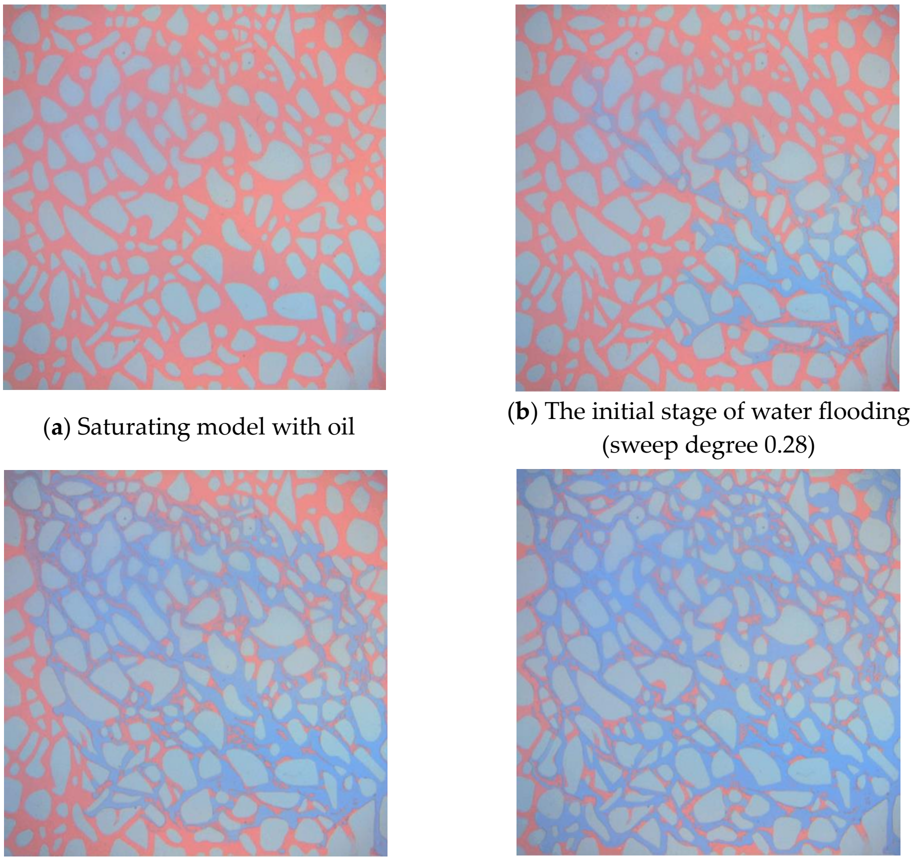

(**a**) Saturating model with oil (**b**) The initial stage of water flooding (sweep degree 0.28) (**c**) The middle stage of water flooding (sweep degree 0.66) (**d**) The late stage of water flooding (sweep degree 0.97)

Figure 6. Water flooding process of the basic model.

4.1.2. Water Flooding Mechanism on the Microscale

Based on the experimental model and experimental parameters, the experimental water flooding characteristics and the formation of the remaining oil are mainly due to the jet filtration effect, flow around effect, penetration effect, and stripping effect of the injected water, the simulation of the wall-attached flow of oil, and the jamming effect of the rock skeleton. The microscopic water flooding mechanism is as follows:

① Jet filtration effect: The injected water advances along the connection between the inlet and outlet of the microscopic model to form the main stream line of flooding. The injected water advances fastest in this direction and forms a dominant channel. The main reasons for this phenomenon are the small size of the sample and the surface tension. The jet filtration phenomenon in the experimental process is shown in Figure 7.

② Detour flow effect: Compared with the large pore throat area, the jamming stress in the small pore throat area is larger, the displacement resistance is larger, and the injected water will preferentially select the large pore throat area with a smaller jamming stress to flow. The flow effect during the experiment is shown in Figure 7.

③ Penetration effect: When the driving force of the simulated oil and the capillary force are far greater than the resistance composed of the viscous force between the crude oil and the displacement fluid and the maximum static friction force between the oil and the rock, the displacement fluid breaks through rapidly, and the simulated oil is displaced to form a channel. This phenomenon mainly occurs in areas with a larger pore throat radius or in areas where the pore throat radius gradually increases. The penetration effect in the experimental process is shown in Figure 7.

④ Pore wall pressing flow effect: The model skeleton in this experiment is lipophilic. The displacement force, composed of capillary force and driving force, is greater than the viscous force between crude oil and displacement fluid and less than the maximum static friction force between crude oil and rock. This leads to the injection of water to displace the simulated oil in the middle of the pore throat, and the crude oil remaining on the pore throat wall exists in the form of a film. The adherent flow of the simulated oil during the experiment is shown in Figure 7.

⑤ Breaking effect: In the process of water flooding, the simulated oil enters the pore throat from the large pore throat to the pore throat with a smaller radius. The capillary force as the driving force of displacement is affected by the jamming effect and becomes the displacement resistance, which makes the driving force of displacement decrease and the displacement resistance increase, resulting in the original continuous oil flow plunger or large oil droplets being blocked. The blocking effect during the experiment is shown in Figure 7.

⑥ Exfoliation effect: Due to the increase in displacement multiples, after the front end of the injected water is in contact with the surface of the simulated oil and rock particles, the simulated oil is stripped off the surface of the hole wall and driven by the driving force of the oil displacement. The stripping effect in the experimental process is shown in Figure 7.

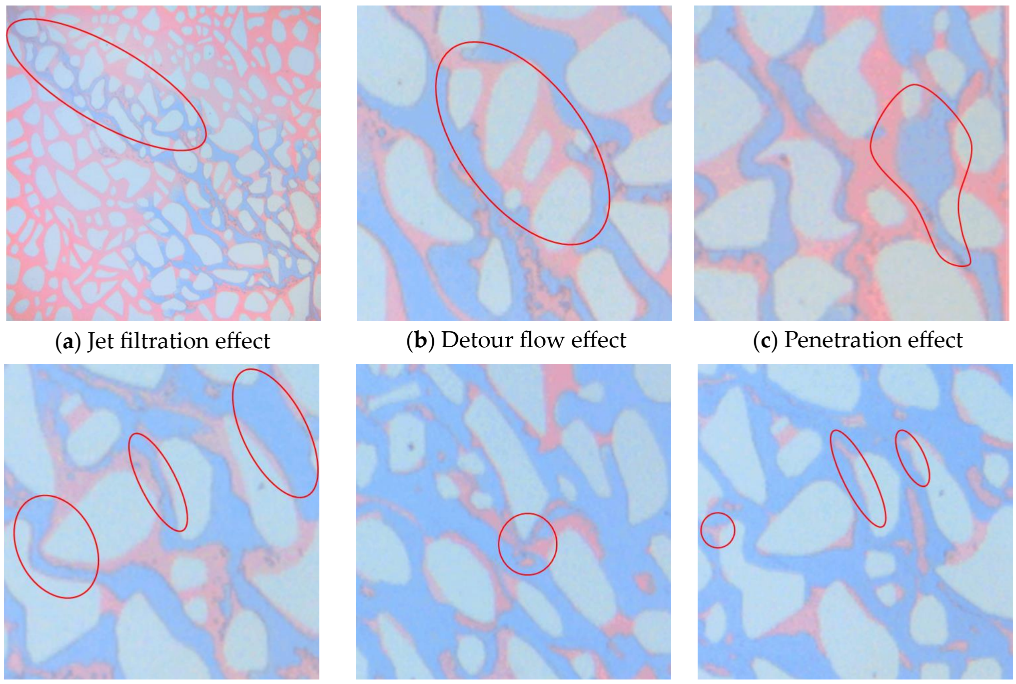

(**a**) Jet filtration effect (**b**) Detour flow effect (**c**) Penetration effect

(**d**) Pore wall pressing flow effect (**e**) Breaking effect (**f**) Exfoliation effect

Figure 7. Water flooding mechanism.

4.2. Microscopic Remaining Oil Types and Evolution Law

4.2.1. Microscopic Remaining Oil Types

According to the experimental results, the microscopic remaining oil in this experiment can be divided into the following five categories: bound continuous flake and porous remaining oil, semi-bound film-like remaining oil, discrete strip and drip remaining oil. Different microscopic remaining oil types are shown in Figure 8, and the specific classification criteria are shown in Table 4.

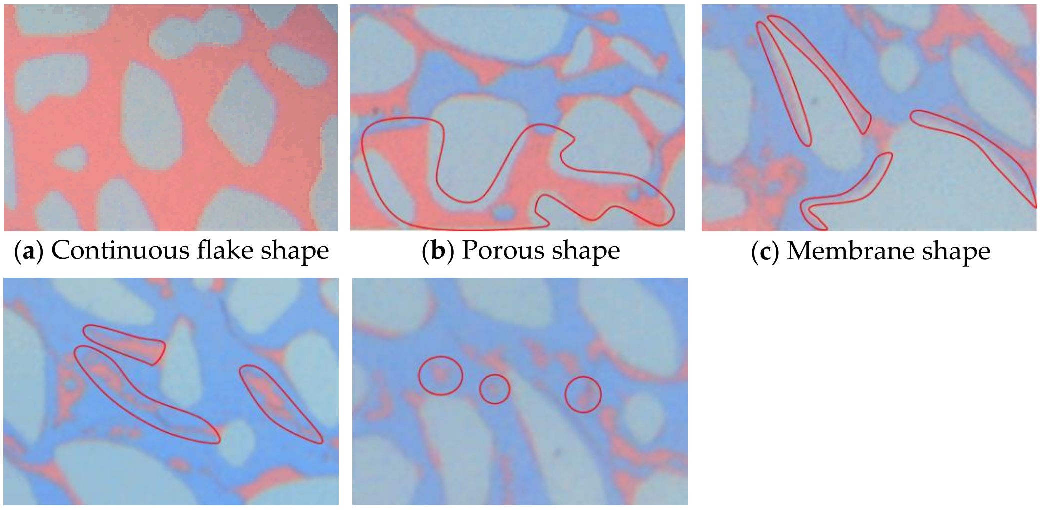

(**a**) Continuous flake shape (**b**) Porous shape (**c**) Membrane shape (**d**) Striped shape (**e**) Drip shape

Figure 8. Different types of microscopic remaining oil.

Table 4. The classification of microscopic remaining oil.

Occurrence Type	Microscopic Remaining Oil Types	Occurrence Location	Contact Ratio	Aspect Ratio	Shape Factor	Pore-Throat Number
Capture	Continuous flake shape	Pore, throat	≥0.5	/	<0.33	>5
	Porous shape	Pore, throat	≥0.5	/	<0.33	≤5
Half capture	Membrane shape	Particle surface	≤0.5	≥2	<0.33	/
Discrete	Striped shape	Pore, throat	=0	≥2	<0.33	/
	Drip shape	Pore	=0	≤2	0.33~0.67	/

4.2.2. Microscopic Remaining Oil Evolution Law

In the process of water flooding, the main types of remaining oil in each stage change with the change in injection volume, which is mainly reflected in the transformation from bound remaining oil to discrete remaining oil. As shown in Figure 9 (the red color in the diagram represents oil and the blue color represents water), the specific transformation processes are as follows:

① In the early stages of water flooding, most of the area has not been effectively used, mainly with contiguous residual oil.
② Due to the penetration effect, the continuous flake residual oil is divided into porous residual oil by the injected water.
③ The displacement of crude oil in the middle of the pores is relatively clean, and there is a large viscous force between the rock wall and the crude oil, forming a film-like remaining oil.
④ With the increase in displacement ratio, the stripping effect of injected water makes the membrane residual oil change to the striped residual oil.
⑤ Due to the blocking effect of pore throat and jamming effect, the striped remaining oil is divided into drip-shaped remaining oil.

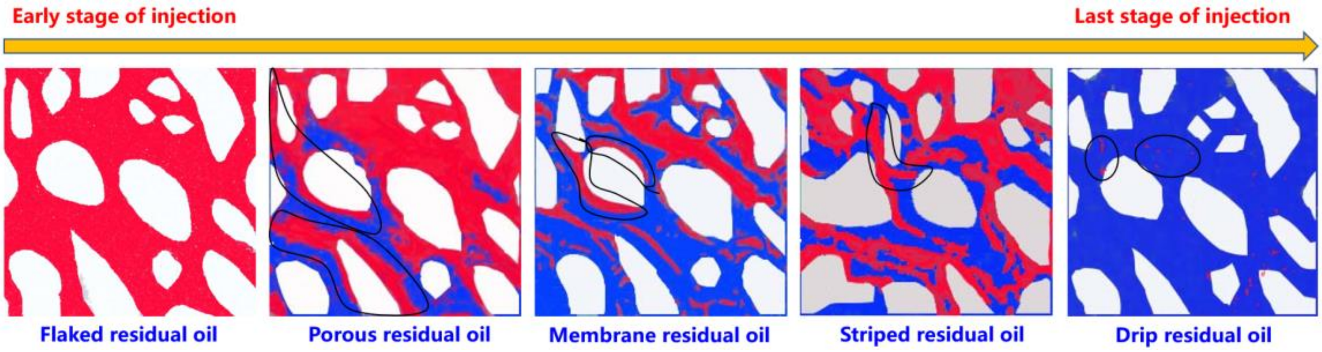

Figure 9. Microscopic remaining oil evolution law.

4.3. The Main Controlling Factors of Different Types of Remaining Oil

4.3.1. Microfluidic Experiments with Different Crude Oil Viscosity

The basic experiment in Section 4.1 uses the simulated oil viscosity of 20 mPa·s, which is a medium-high-viscosity oil. Its water flooding characteristics and remaining oil types are different from the light oil model. This study will carry out the water flooding experiment with a simulated oil viscosity of 2 mPa·s and compare and analyze the differences in water flooding characteristics and microscopic remaining oil under different crude oil viscosities.

Control experiment 1: Simulated oil viscosity of 2 mPa·s; injected water viscosity of 1 mPa·s; injection speed of 0.02 mL/min. In the early stages of water flooding, the injected water extends slowly from the injection end in a fan shape, and the jet filtration phenomenon is not obvious, which is similar to piston displacement. In the middle stage of water flooding, the small jet filtration of the fan-shaped water flooding front appears on the injection-production line, and the water flooding front first reaches the outlet end, and the affected area increases with the increase in the displacement multiple. At the end of water flooding, the shape and content of the remaining oil basically do not change with the increase in displacement multiples.

By comparing and analyzing the types and contents of remaining oil at the end of the two groups of experimental water flooding, it can be found that the remaining oil of the low-viscosity model is mainly composed of continuous, porous, membrane-like, and drip-like remaining oil. The jet filtration phenomenon of the medium-high-viscosity oil model is serious, and the dominant channel of water flooding is formed in the main stream line, and the swept area of injected water is small. The jet filtration phenomenon of the light oil model is weak, the displacement is more uniform, and the streamline distribution is more dispersed. The experimental results are shown in Figure 10 (the red color in the diagram represents oil and the blue color represents water).

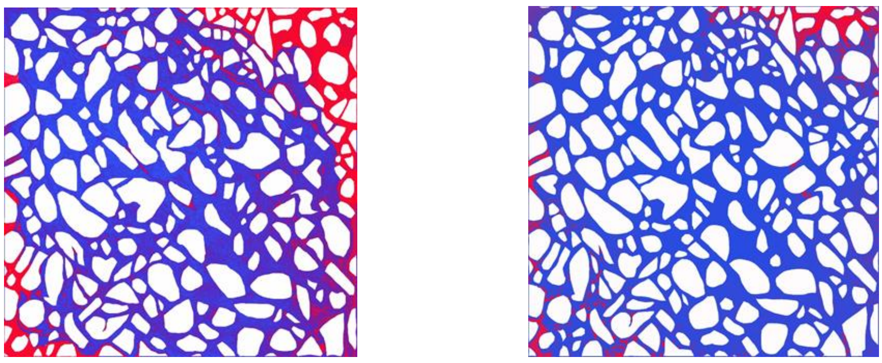

(**a**) Medium-high-viscosity oil model result (**b**) Light oil model result

Figure 10. Oil-water distribution at the end stage of water flooding under different viscosities.

The remaining oil content of the two models is mainly composed of the continuous sheet and porous types. In addition to these two types of remaining oil, the striped and membrane remaining oil account for a relatively high proportion in the medium-high-viscosity oil model. In the light oil model, the remaining oil of the droplet and membrane types is relatively high. The different types of microscopic remaining oil in the two groups of experiments are shown in Figure 11.

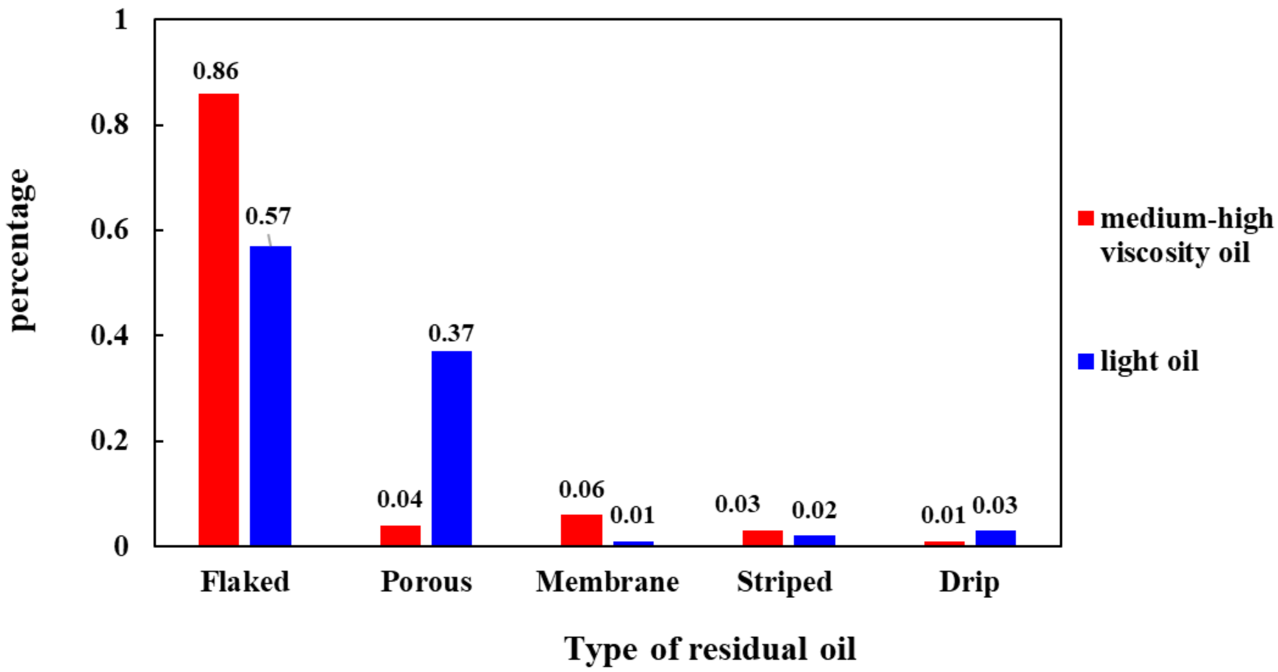

Figure 11. The proportion of different types of microscopic remaining oil under different viscosities models.

The viscosity of crude oil has the greatest influence on the continuous sheet and the porous remaining oil. The decrease in contiguous residual oil was as high as 33.7%. The decrease in the oil-to-water mobility ratio leads to the transformation of continuous sheet remaining oil to porous remaining oil. The greater the viscosity of crude oil, the greater the oil mobility ratio, the more serious the jet filtration phenomenon in the water flooding process, and the lower the oil displacement efficiency. In this study, the oil displacement efficiency of the light oil model is 7.2% higher than that of the medium-high-viscosity oil model.

4.3.2. Microfluidic Experiments under Different Water Injection Intensities

Control experiment 2: Simulated oil viscosity of 20 mPa·s; injected water viscosity of 1 mPa·s; injection speed of 0.06 mL/min. The water flooding law of the model is similar to that of the low-speed water injection model. In the early stages of water flooding, the injected water flows faster along the line between injection and production wells, and the outlet end sees water quickly. In the middle stage of water flooding, the swept area of injected water diffuses from the main stream line to both sides, and the diffusion rate is greater than the low-speed model at the same stage. At the end of water flooding, the shape and content of the remaining oil basically do not change with the increase in displacement multiples.

At the same water injection PV number at the end of water flooding, the swept area of the high-speed water injection model is larger. High-speed water injection has little effect on the continuous residual oil, and part of the membrane-like residual oil is stripped to transform into discrete strip-like and drip-like residual oil. The experimental results are shown in Figure 12 (the red color in the diagram represents oil and the blue color represents water), and the remaining oil of each type is shown in Figure 13.

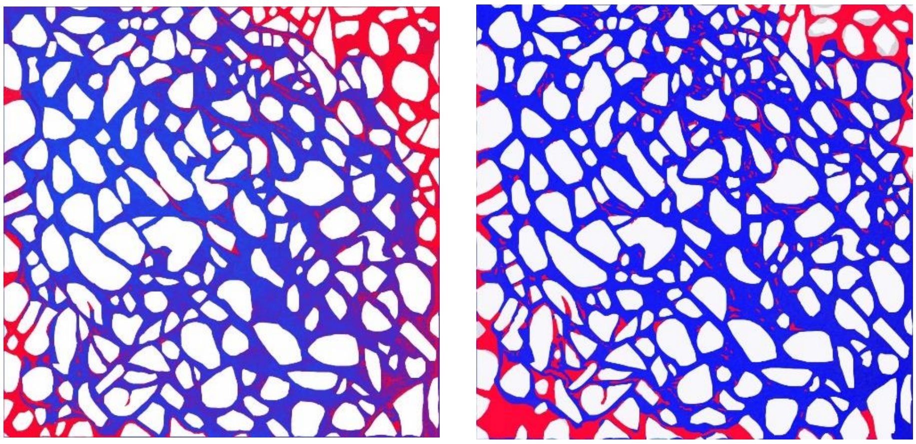

(**a**) Low-speed water injection (**b**) High-speed water injection model

Figure 12. Oil/water distribution at the end stage of water flooding at different water injection rates.

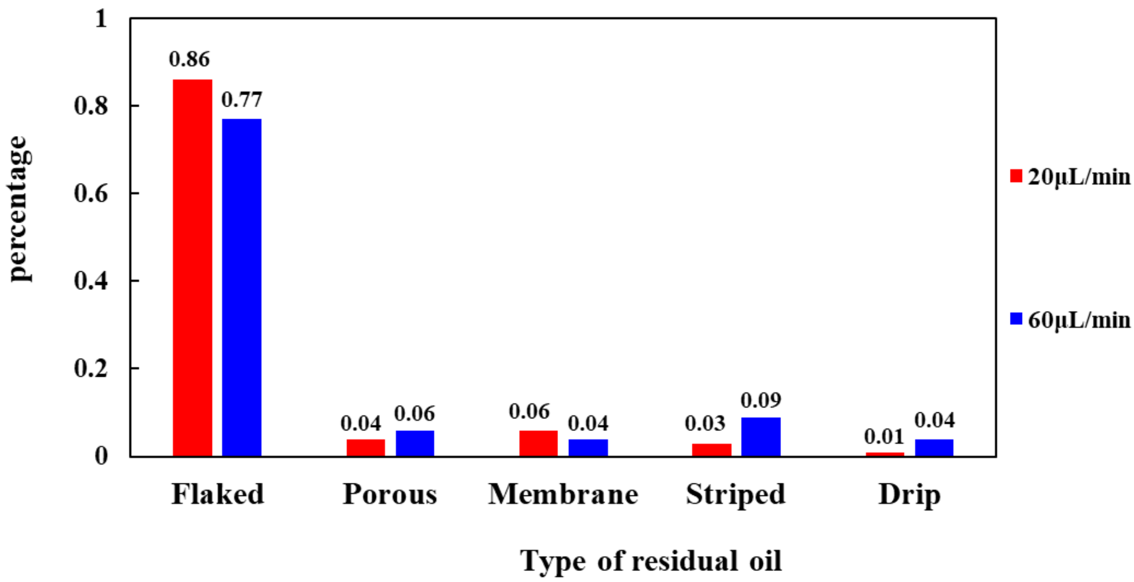

Figure 13. The proportion of different types of microscopic remaining oil under different water injection rates.

The water injection rate has a great influence on the membrane, striped, and drip remaining oil. The high-speed erosion of the injected water stripped the membrane remaining oil, resulting in a decrease in membrane residual oils of up to 33.3%. And the membrane residual oil transformed into strip and drip remaining oil. The greater the water injection rate, the greater the number of capillaries, the stronger the oil displacement power, and the greater the oil displacement efficiency. In this study, the capillary number of the low-speed water injection model is $Nc_1 = 1.1 \times 10^{-3}$, and the capillary number of the high-speed water injection model is $Nc_2 = 3.3 \times 10^{-3}$. The oil displacement efficiency of the high-speed water injection model is 4.8% higher than that of the low-speed water injection model.

The experiments involved in this study are reproducible, and the results obtained after several repetitions of the experiments show that the specific morphology of the residual oil obtained from each experiment is slightly different; however, the pattern embodied is consistent, and the data discrepancy is within 10%. The experiments listed in this paper are representative.

5. Conclusions

In this paper, in order to investigate the microscopic water drive mechanism and the main controlling factors of different types of residual oil during the water drive development of high-porosity and high-permeability medium-high-viscosity oil reservoirs, we carried out a microscopic drive experiment in high-porosity and high-permeability reservoirs. The following conclusions can be drawn from the comparative analysis of the experimental results:

(1) Microscopic water drive characteristics: Injecting water in the form of filaments protruding along the connecting line between injection and production wells. As the water drive proceeds, the injected water spreads along the main flow line to the unrippled areas on both sides, and the extent of injected water rippling reaches almost 100% after the water breakthrough has happened at the export side. At the end of the water drive, the residual oil morphology and content hardly vary with the injection volume.

(2) Microscopic water drive mechanism: The formation of microscopic residual oil is mainly due to jet filtration, penetration, bypassing, advective flow, stripping of the injected water, and seizing of the rock skeleton.

(3) Microscopic residual oil classification: Based on the location, contact ratio, aspect ratio, shape factor, and number of pores and throats of residual oil, the residual oil was categorized into five types, i.e., contiguous residual oil, porous residual oil, membrane residual oil, strip residual oil, and drip residual oil.

(4) Microscopic residual oil evolution pattern: As the water drive proceeds, the residual oil changes along the sequence of continuous sheet, porous, membrane, strip, and drip, in which the strip residual oil includes two kinds of direct formation and transformation of membrane residual oil.

(5) Analysis of the main controlling factors of different types of residual oil: The main controlling factor for contiguous and porous residual oil is crude oil viscosity. The main reason is that the oil-water flow rate ratio is large, resulting in a serious jet filtration phenomenon, and the injection water forms a dominant seepage channel, leading to the existence of contiguous pieces of residual oil that are not effectively utilized. The main controlling factor for membrane, strip, and drip residual oil is injection intensity. High-rate water injection elevates the number of capillary tubes, which increases the driving force and transforms the membrane residual oil into strip and drip residual oil.

Author Contributions: Conceptualization, P.J. and Y.L.; methodology, P.J.; software, Y.L., M.L. and H.F.; validation, Y.L., M.L. and C.P.; formal analysis, P.J.; investigation, P.J. and Y.L.; data curation, Y.L. and H.F.; writing—original draft preparation, Y.L. and C.P.; writing—review and editing, P.J. and L.C.; supervision, P.J. and L.C.; project administration, P.J.; funding acquisition, P.J. and L.C. All authors have read and agreed to the published version of the manuscript.

Funding: This research was partially funded by the National Natural Science Foundation of China (No. 52004307). We would further like to thank the financial support of the Science and technology project of CNPC (No. ZLZX2020-02-04).

Conflicts of Interest: The authors declare no conflict of interest. The funders had no role in the design of the study, the collection, analysis, or interpretation of data, the writing of the manuscript, or the decision to publish the results.

References

1. Yue, P.; Qu, S.M.; Li, F.H.; Wang, Q.L.; Zhang, L.; Luo, X.; Feng, X.; Ren, Y.W. Characteristics of residual oil distribution in high-porosity, high-permeability, high-water-content thick oil reservoirs and the main controlling factors of utilization. *Unconv. Oil Gas* **2023**, *10*, 33–42.
2. Chatenever, A.; Calhoun, J.C., Jr. Visual examinations of fluid behavior in porous media—Part I. *J. Pet. Technol.* **1952**, *4*, 149–156. [CrossRef]
3. Guo, S.P.; Huang, Y.Z.; Zhou, J. *Micro-Mechanisms of Physicochemical Seepage*; Science Press: Beijing, China, 1990.

4. Li, J.J.; Su, H.; Jiang, H.; Yu, F.; Liang, T.; Zhao, Y.; Gao, Y.; Hossein, H. Application of microfluidic modeling in oil and gas field development. *J. Pet. Sci.* **2018**, *3*, 284–301.
5. Xu, K.; Liang, T.; Zhu, P.; Qi, P.; Lu, J.; Huh, C.; Balhoff, M. A 2.5-D glass micromodel for investigation of multiphase flow in porous media. *Lab. Chip.* **2017**, *17*, 640–646. [CrossRef] [PubMed]
6. Ginger, R.; Abedini, A.; Yang, H.; Sanders, A. Visualization of Flowback Aid Mechanisms Utilizing a Microfluidic Pore-Scale Device. In Proceedings of the International Conference and Exhibition on Formation Damage Control, SPE-199269-MS, Lafayette, LA, USA, 12 February 2020.
7. Yuan, S.; Liang, T.B.; Zhou, F.J.; Liang, X.; Yu, F.; Li, J. A Microfluidic Study of Wettability Alteration Rate on Enhanced Oil Recovery in Oil-Wet Porous Media. In Proceedings of the Abu Dhabi International Petroleum Exhibition & Conference, SPE-197715-MS, Abu Dhabi, United Arab Emirates, 11 November 2019.
8. Khayrullin, M.M.; Zakirov, T.R.; Grishin, P.A.; Shilov, E.D.; Bukatin, A. Methods for Studying Two-Phase Flows in Porous Media: Numerical Simulation and Experiments on Microfluidics Chips. In Proceedings of the Russian Petroleum Technology Conference, SPE-202022-MS, Virtual, 26 October 2020.
9. Zhou, J.; Xue, H.; Zheng, D.W.; Liu, X.W. Seepage Mechanism of Water-driven Oil in Fractured Reservoirs. *J. Chongqing Univ. Nat. Sci. Ed.* **2000**, *S1*, 65–67.
10. Chen, Y.Y.; Sun, L.; Tian, T.H.; Pan, Y.; Dong, W.J.; Liu, Y.Z. Visual modeling of fractured carbonate reservoirs for water-driven oil experiments. *Fault Block Oil Gas Fields* **2012**, *19*, 92–94.
11. Chen, M. *Quantitative Characterization of Microscopic Seepage Mechanism in Water-Driven Reservoirs*; Southwest Petroleum University: Chengdu, China, 2017.
12. Alizadeh, A.H.; Khishvand, M.; Ioannidis, M.A.; Piri, M. Multi-scale experimental study of carbonated water injection: An effective process for mobilization and recovery of trapped oil. *Fuel* **2014**, *132*, 219–235. [CrossRef]
13. Chen, X.L.; Han, H.S.; Li, S.; Yu, H.W. Microscopic characterization of residual oil in CO_2-initiated blind-end pores. *Oil Gas Geol. Recovery* **2020**, *27*, 50–56.
14. Cui, M.L.; Wang, R.; Lv, C.Y.; Lun, Z.M.; Zhao, S.X.; Tang, Y.Q. Microscopic oil drive mechanism of reinjected natural gas drive in high pressure and low permeability reservoirs. *Oil Gas Geol. Recovery* **2020**, *27*, 62–68.
15. Li, J.; Jiang, H.; Wang, C.; Zhao, Y.; Gao, Y.; Pei, Y.; Wang, C.; Dong, H. Pore-scale investigation of microscopic remaining oil variation characteristics in water-wet sandstone using CT scanning. *J. Nat. Gas Sci. Eng.* **2017**, *48*, 36–45. [CrossRef]
16. Wang, C.; Jiang, H.Q.; Ma, M.Q.; Xu, F.; Yu, F.W.; Zhao, Y.Y.; Li, J.J. Research on the change rule of residual oil flow state at pore scale based on microfluidic modeling. *Pet. Sci. Bull.* **2020**, *5*, 376–391.
17. Li, Q.; Zhang, C.; Yang, Y.D.; Ansari, U.; Han, Y.; Li, X.; Cheng, Y. Preliminary experimental investigation on long-term fracture conductivity for evaluating the feasibility and efficiency of fracturing operation in offshore hydrate-bearing sediments. *Ocean Eng.* **2023**, *281*, 114949. [CrossRef]
18. Li, Q.; Zhao, D.; Yin, J.; Zhou, X.; Li, Y.; Chi, P.; Han, Y.; Ansari, U.; Cheng, Y. Sediment Instability Caused by Gas Production from Hydrate-bearing Sediment in Northern South China Sea by Horizontal Wellbore: Evolution and Mechanism. *Nat. Resour. Res.* **2023**, *32*, 1595–1620. [CrossRef]